

SAR PROCESSING FOR PROFILE RECONSTRUCTION AND CHARACTERIZATION OF DIELECTRIC OBJECTS ON THE HUMAN BODY SURFACE

Borja Gonzalez-Valdes^{1, *}, Yuri Álvarez², José A. Martínez¹, Fernando Las-Heras², and Carey M. Rappaport¹

¹The Gordon CenSSIS/ALERT Center of Excellence, Northeastern University, Boston, MA 02115, USA

²Department of Electrical Engineering, Universidad de Oviedo, Campus Universitario, Gijón, Asturias 33203, Spain

Abstract—Contour reconstruction and accurate identification of dielectric objects placed on a conducting surface are the aims of the millimeter-wave Synthetic Aperture Radar (SAR) imaging processing system presented in this paper. The method uses multiple frequencies, multiple receivers and one transmitter in a portal-based configuration in order to generate the SAR image. Then, the information in the image is used to estimate the contour of the body under test together with the permittivity of the dielectric region. The results presented in this paper are based on synthetic scattered electromagnetic field data generated using an accurate Finite-Difference Frequency-Domain (FDFD)-based model and inversion based on a fast SAR inversion algorithm. Representative examples showing the good behavior of the method in terms of detection accuracy are provided.

1. INTRODUCTION

Screening systems are becoming increasingly important in many scenarios. Traditional screening methods use X-rays for baggage inspection and metal detectors for personnel inspection. Metal detectors are not able to detect non-metallic threats such as explosives. This limitation together with others such as scanning speed, detection of small objects (i.e., resolution) and overall cost of the system must be addressed in the next generation of personnel scanning systems developed to detect concealed threats or contraband.

Received 6 February 2013, Accepted 6 March 2013, Scheduled 22 March 2013

* Corresponding author: Borja Gonzalez-Valdes (b.gonzalezvaldes@neu.edu).

A wide range of electromagnetic imaging techniques have been applied in order to detect and identify objects placed under clothing [1–10]. Terahertz waves [8], and X-ray [9, 10] have shown their feasibility. However, terahertz electronics are not yet commercially available and are quite expensive so imaging must be done with mechanically scanned reflectors rather than arrays, while X-ray based systems make use of ionizing emissions, which though of very low dose, are not acceptable to the public.

Millimeter-wave radar provides a trade-off solution between accuracy and cost. Considerable progress has been made for reconstructing human body surface geometry for security applications [3]. Recently, the possibility of using Synthetic Aperture Radar (SAR) processing from scattered field measurements to rapidly and effectively reconstruct the shape of the human body torso with attached objects concealed under clothing has been studied [1, 4, 6].

A different approach characterizes the material under study in order to find possible threats such as explosives or contraband. In this field, penetrating X-rays [11], terahertz waves [12–14], neutron analysis [15] and Nuclear Quadrupole Resonance (NQR) [16] have been proposed. These systems can detect some dielectric materials properties but in general, they are not able to determine the shape of the object and are not designed for its integration in the portal-based systems used for personnel inspection.

A much more versatile detection system could be built by adding to the shape detection component the ability to identify material properties. In this work we present an innovative millimeter wave-based SAR system able to determine the shape and constitutive electrical parameters of dielectric objects placed or embedded on the surface of a conductor. The algorithm takes advantage of the phenomenon that in high frequencies the human body behaves as a good conductor while most dielectrics will allow energy penetration. In these conditions, information on both the shape and the relative permittivity of the dielectric bodies can be extracted from the SAR image.

The proposed system is configured for multiple frequencies, multiple receivers, and one transmitter in a portal-based configuration, as presented in Fig. 1. The characterization technique is described with detail in Section 2; Section 3 presents an application example to demonstrate the feasibility of the method, whereas validation with measurements is shown in Section 4.

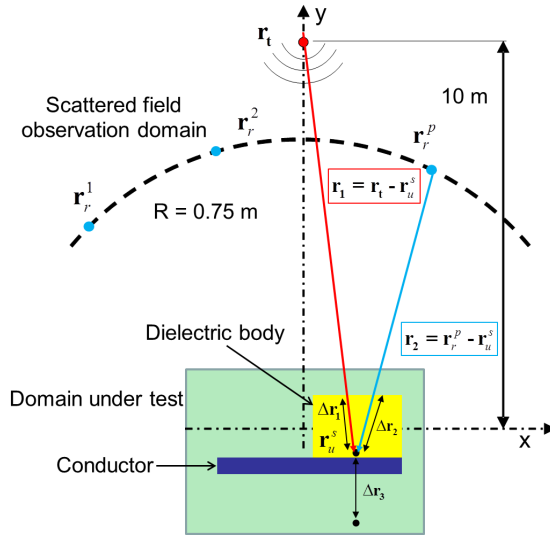


Figure 1. Proposed measurement setup for detecting and identify concealed dielectric objects placed onto the human body torso.

2. EFFECT OF THE DIELECTRIC CONSTANT IN THE SAR IMAGE

In this section we present the SAR processing method to reconstruct object dielectric constant. More details on the implementation of the proposed SAR reconstruction can be found in previous work [5, 6].

A general scheme of the two dimensional proposed configuration is presented in Fig. 1. For this configuration, the field $\mathbf{E}(f^l, \mathbf{r}_t, \mathbf{r}_r^p)$ scattered by the domain under test when transmitting from a point \mathbf{r}_t with the frequency f^l is measured at the p -th point placed in \mathbf{r}_r^p . For a given two-dimensional reconstruction domain, the SAR image of the pixel placed in \mathbf{r}_u^s is calculated from the field as [1, 5]:

$$I(\mathbf{r}_u^s) = \sum_{l,p} \mathbf{E}(f^l, \mathbf{r}_t, \mathbf{r}_r^p) e^{+j\Phi(f^l, \mathbf{r}_t, \mathbf{r}_r^p, \mathbf{r}_u^s)} \quad (1)$$

If the wave is propagating in free space, the phase shift in (1) can be calculated as:

$$\Phi(f^l, \mathbf{r}_t, \mathbf{r}_r^p, \mathbf{r}_u^s) = \phi_1 + \phi_2 \quad (2)$$

$$\phi_1 = k_0^l |\mathbf{r}_1| = k_0^l |\mathbf{r}_t - \mathbf{r}_u^s|, \quad \phi_2 = k_0^l |\mathbf{r}_2| = k_0^l |\mathbf{r}_r^p - \mathbf{r}_u^s|$$

where $k_0^l = 2\pi f^l \sqrt{\mu_0 \epsilon_0}$ is the wave number in free space at frequency

f^l ; $\mu_0 = 4\pi \times 10e^{-7}$ [H/m] and $\epsilon_0 = 8.854 \times 10e^{-12}$ [F/m] are the free space permeability and permittivity, respectively. The terms in Equation (2) correspond to the propagation from the transmitter to the pixel placed at \mathbf{r}_u^s and from that pixel to the p -th receiver.

The SAR image generated by this technique will be proportional to the electric currents at the pixel. If the material placed in the pixel under study is a good conductor (i.e., no energy penetrates into the material under test) the reconstruction of the currents proposed in Equation (1) will estimate the position of the currents in the domain, and thus the object shape. The accuracy is given by the resolution of the radar system [17]. However, in the case of dielectric materials, a certain amount of energy, proportional to the transmission coefficient between the air and the dielectric, will propagate through the material [1]. The wavenumber for this propagating field will be given by $k_d^l = 2\pi f^l \sqrt{\mu_0 \epsilon_r \epsilon_0}$ where ϵ_r is the relative dielectric constant of the dielectric material.

The speed of propagation in the dielectric is reduced with respect to the speed in the air. In the case of dielectric bodies placed on good conductors such as the human body, this delayed incident field will propagate through the dielectric to the conducting skin and reflect back to the observation points after crossing the dielectric body with reduced speed a second time. The SAR image of a point placed on the surface of the obstructed conductor, \mathbf{r}_u^s in Fig. 1 will be given by:

$$I(\mathbf{r}_u^s) = \sum_{l,p} \mathbf{E} \left(f^l, \mathbf{r}_t, \mathbf{r}_r^p \right) e^{+jk_0^l(|\mathbf{r}_1| - |\Delta\mathbf{r}_1| + |\mathbf{r}_2| - |\Delta\mathbf{r}_2|) + jk_d^l(|\Delta\mathbf{r}_1| + |\Delta\mathbf{r}_2|)} \quad (3)$$

The relationship between the phase terms of Equations (1) and (3) will provide the following phase term for a given l -frequency and p -position:

$$\begin{aligned} \frac{I(\mathbf{r}_u^s)|_{dielectric}^{l,p}}{I(\mathbf{r}_u^s)|_{Freespace}^{l,p}} &= \frac{e^{+jk_0^l(|\mathbf{r}_1| - |\Delta\mathbf{r}_1| + |\mathbf{r}_2| - |\Delta\mathbf{r}_2|) + jk_d^l(|\Delta\mathbf{r}_1| + |\Delta\mathbf{r}_2|)}}{e^{+jk_0^l(|\mathbf{r}_1| + |\mathbf{r}_2|)}} \\ &= e^{+jk_0^l(-|\Delta\mathbf{r}_1| - |\Delta\mathbf{r}_2|) + jk_d^l(|\Delta\mathbf{r}_1| + |\Delta\mathbf{r}_2|)} \\ &= e^{-jk_0^l(|\Delta\mathbf{r}_1| + |\Delta\mathbf{r}_2|)(1 - \sqrt{\epsilon_r})} \end{aligned} \quad (4)$$

The phase term introduced in the reconstruction of Equation (4) will displace the position of the currents in the SAR image to a distance $|\Delta\mathbf{r}_3|$ that will add the currents in phase when:

$$\begin{aligned} \sum_{l,p} e^{2k_0^l|\Delta\mathbf{r}_3|} &= \sum_{l,p} e^{-jk_0^l(|\Delta\mathbf{r}_1| + |\Delta\mathbf{r}_2|)(1 - \sqrt{\epsilon_r})} \\ &\Rightarrow 2|\Delta\mathbf{r}_3| = (|\Delta\mathbf{r}_1| + |\Delta\mathbf{r}_2|)(\sqrt{\epsilon_r} - 1) \end{aligned} \quad (5)$$

This effect is not taken into account in the conventional SAR formulation in Equation (1) since the wavenumber in free space is used to reconstruct the currents for every pixel and the resulting image is inaccurate. However, certain features of the image can be used to identify the dielectric constant of the material under test, as shown in next section. The use of the free space wavenumber in the SAR processing will create the effect of displacing the reflection on the obstructed surface of the conductor and amount $|\Delta \mathbf{r}_3|$ in approximately the direction of the incident wave. Since this displacement is directly proportional to the dielectric permittivity and size, its identification in the SAR image will provide information on the dielectric body permittivity and size.

3. SIMULATION RESULTS

To illustrate the capabilities of the inverse method for the reconstruction of the shape and the permittivity of dielectric objects placed on the surface of conductors, one representative application example is considered in this section. A multi-frequency radar system will be used with 15 GHz bandwidth from 55 to 70 GHz in 500 MHz-steps (i.e., a bandwidth of 24% with respect to the center frequency, 62.5 GHz). The direct problem is simulated using a Frequency Domain Finite Differences (FDFD) algorithm [18]. This method is selected because of its accuracy in modeling the interaction between general dielectric objects.

A canonical example is considered to demonstrate the method's behavior. The example consists of two pure dielectric objects placed on 1-cm thick skin slab (Fig. 2). Due to its high water content, a

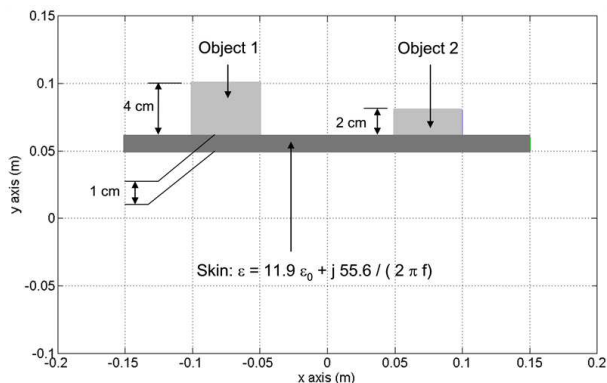


Figure 2. Geometry and constitutive parameters of the example.

1 cm thickness of skin absorbs all the wave transmitted through its top boundary, and as such is sufficient to model a full thickness human body volume. The problem will be analyzed for different values of the relative dielectric constant of the bodies to show the behavior of the SAR system in terms of permittivity and shape identification.

The selected geometry is illuminated with an incident wave that behaves almost as the manufactured Blade-Beam reflector antenna used as transmitter in [4]. This behavior is achieved by means of a cylindrical wave centered at $(x, y) = (0, 10)$ m. The backscattered field on a 180° arc, placed $R = 0.75$ m away from the geometry-under-test is calculated. The sampling rate is $\Delta = 1.25^\circ$, which is about 0.5λ at the center frequency.

From the scattered field, the equivalent currents are retrieved on a 0.4×0.25 m domain, sampled each $\Delta S = (0.1\lambda)^2$. The retrieved SAR images for $\epsilon_r = 1.5, 3, 6$ and 15 are plotted in Figs. 3 to 6. Several cuts in the line perpendicular to the dielectric center are presented to show the maximum reflection points for the different dielectric objects.

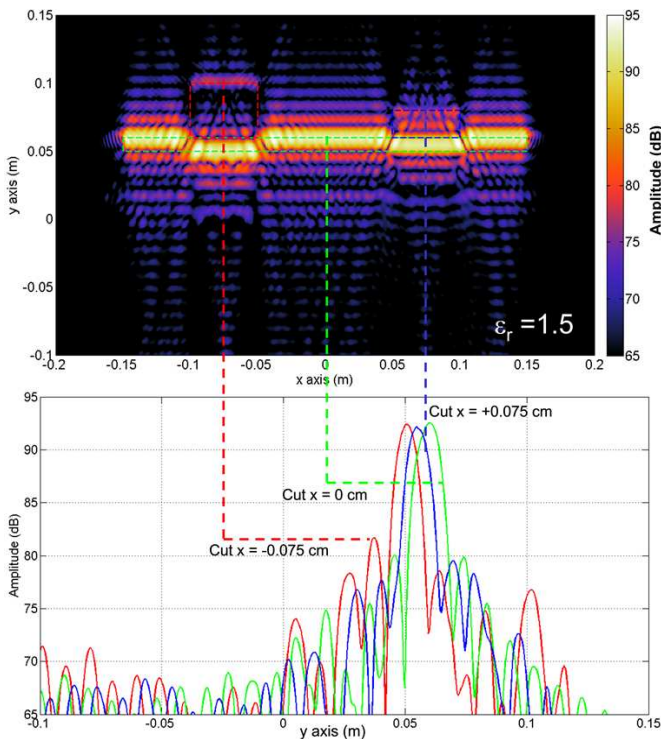


Figure 3. SAR image (top) and cuts along y -axis for $\epsilon_r = 1.5$.

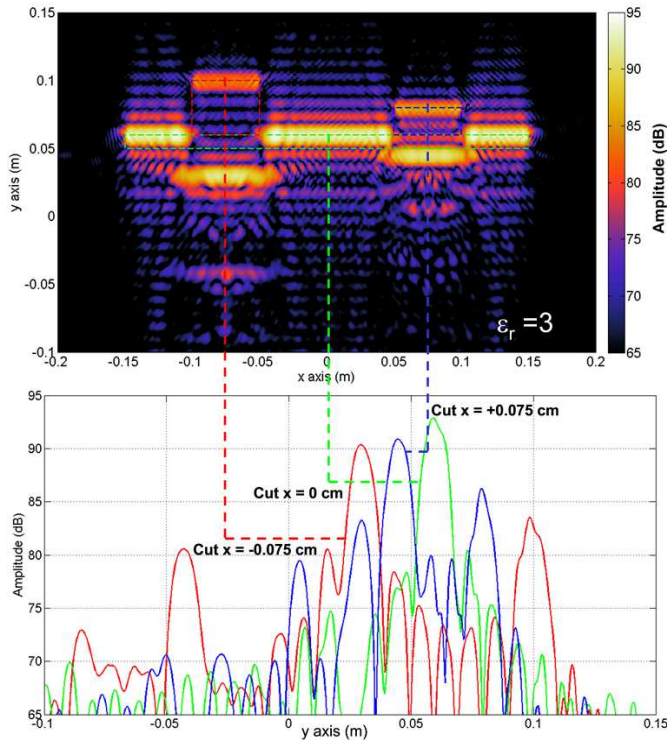


Figure 4. SAR image (top) and cuts along y -axis for $\epsilon_r = 3$.

From the retrieved SAR images, it can be observed that the maximum amplitude values correspond to the positions where the incident field reflects from the skin and dielectric objects surfaces. The shape of the dielectric-skin interface can be easily identified in all the images. The amplitude of the currents on the dielectric bodies surface is lower for low relative permittivity values due to the fact that almost all the power is transmitted through the dielectric.

The SAR imaging artifact of the second reflection, caused by slower wave propagation in the dielectric object provides information to determine its dielectric constant. The differential distance from the nominal skin surface to the apparent skin surface at the back of the object, d_{echo} is given by:

$$d_{echo} = d_{obj}(\sqrt{\epsilon_r} - 1) \tag{6}$$

where d_{obj} is the distance between the conductive skin and the dielectric surface, ϵ_r the permittivity of the dielectric material, and $d_{obj} \approx |\Delta \mathbf{r}_1| \approx |\Delta \mathbf{r}_2|$ the thickness of the dielectric object. To confirm

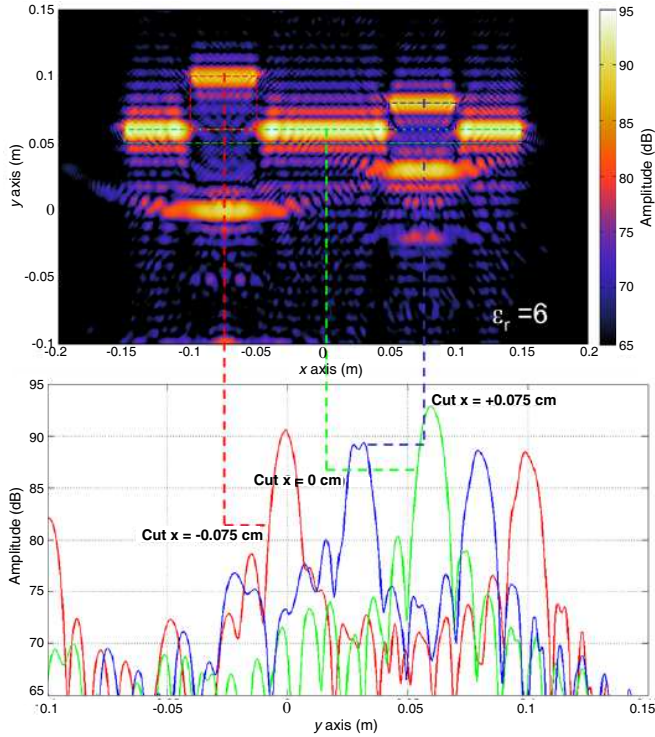


Figure 5. SAR image (top) and cuts along y -axis for $\epsilon_r = 6$.

this behavior, the calculated and measured distances on the SAR images are compared in Fig. 7 for the 2 and 4 cm objects and for different relative permittivity values.

The relative permittivity can be estimated as:

$$\epsilon_{r,est} = \left(1 + \frac{d_{echo}}{d_{obj}} \right)^2 \quad (7)$$

which compares with true values of $\epsilon_r = 1.5, 3, 4.5, 6, 10$ and 15 in Fig. 8.

4. MEASUREMENT RESULTS

In order to validate the simulation results presented in the previous section, a set of experimental measurements have been collected. Since the 60 GHz portal-based measurement setup is still under development and testing [4], preliminary lower frequency measurements have been

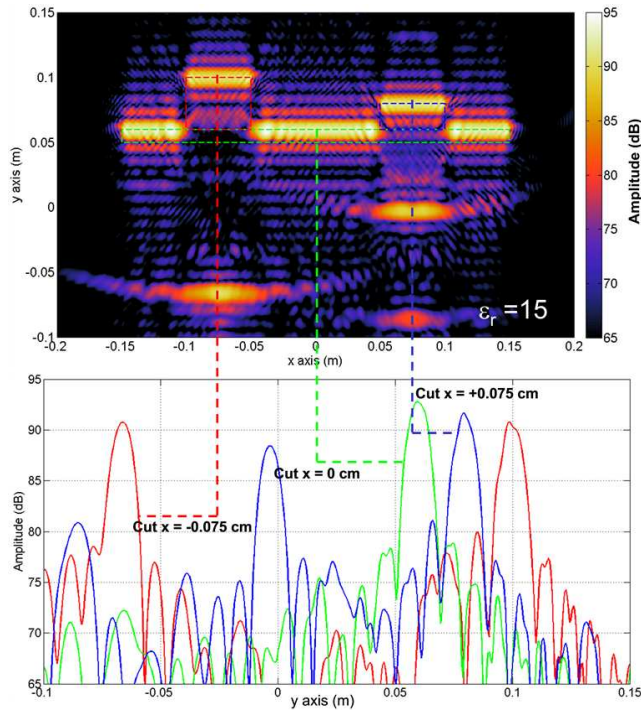


Figure 6. SAR image (top) and cuts along y -axis for $\epsilon_r = 15$.

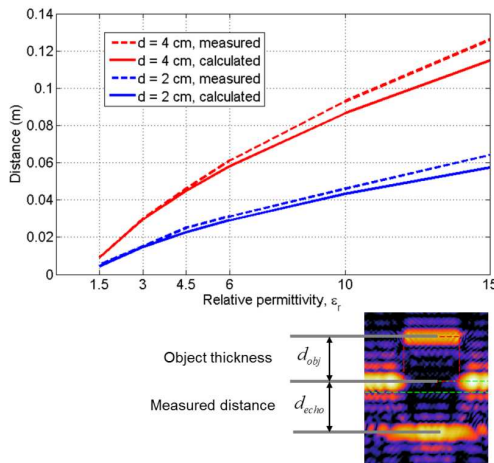


Figure 7. Calculated and measured distance at which the echo due to the reflection between the dielectric and skin interfaces is located.

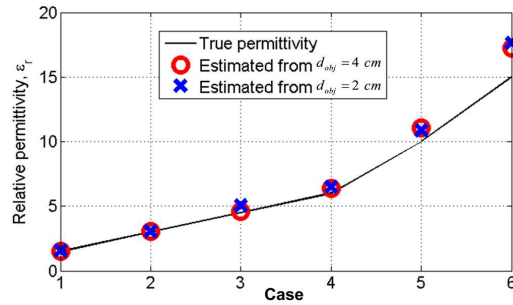


Figure 8. Relative permittivity. Theoretical and estimated from the SAR image distance among echoes.

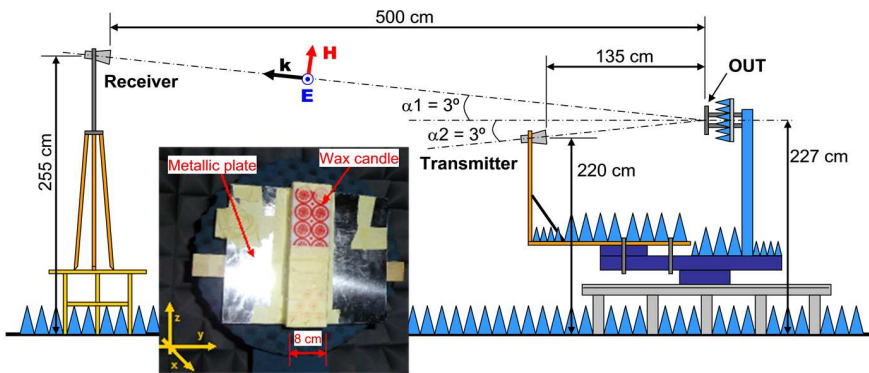


Figure 9. Experimental measurement setup, and photograph of the bent metallic plate with a 8 cm side square wax candle on it.

performed at the spherical range in anechoic chamber of the University of Oviedo. The measurement setup is depicted in Fig. 9. The object-under-test (OUT) is a slightly bent metallic surface that aims to model the human body torso curvature. The dielectric object under test is an 8 cm side square wax candle placed on it.

The frequency range is from 18 to 26 GHz (36% bandwidth), sampled every 500 MHz steps. The field scattered by the OUT has been measured on a 90 degrees arc placed 5 m away of the object, with a sampling rate of $\Delta = 1^\circ$. From the scattered field, the equivalent currents are retrieved on a 0.4×0.225 m domain. To avoid transmitting/receiving antennas blockage, the illumination is tilted 3° with respect to the XY plane, as shown in Fig. 9.

For comparison purposes, the measurement setup has been simulated using the FDFD code [18]. The wax candle is assumed to have a relative permittivity of $\epsilon_r = 2.5$. Simulation results are

depicted in Fig. 10(a). The echoes due to the reflections on the air-dielectric and dielectric-metal interfaces are clearly visible. For this case, $d_{echo} \sim 4$ cm and $d_{obj} = 8$ cm. From Equation (7), the estimated permittivity is 2.3, which is close to the expected value of $\epsilon_r = 2.5$.

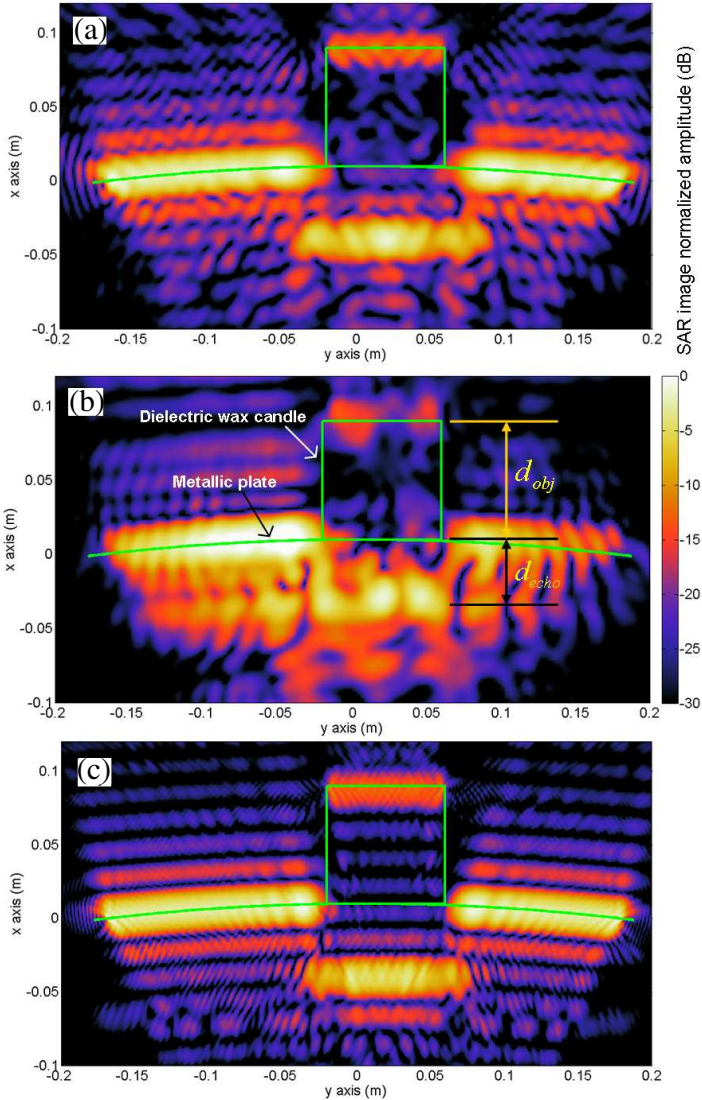


Figure 10. SAR image for a dielectric object placed on a bent metallic plate. (a) Simulations from 18 to 26 GHz. (b) Measurements from 18 to 26 GHz. (c) Simulations from 60 to 68 GHz.

Figure 10(b) presents the SAR imaging results from measured data. It can be appreciated the good agreement between simulated- and measurements-based results: in both cases, the metallic profile, the dielectric-metal interface echo, and the dielectric-air echo are clearly visible, confirming the validity of the method to recover not only the geometry information, but also the permittivity of the wax candle.

Next, these results are extrapolated to the proposed portal-based measurement setup operating frequency band [4]. Fig. 10(c) shows the FDFD simulation of the same geometry with the same 8 GHz bandwidth in the 60 to 68 GHz band, showing results similar to those at lower frequencies (Figs. 10(a) and (b)). This fact proves the feasibility of using millimeter waves for dielectric object identification in the proposed configuration.

5. CONCLUSIONS

A new millimeter-wave SAR image approach to identify the shape and relative permittivity of dielectric objects placed on the body has been presented. The reconstruction is tested using FDFD to simulate the scattered field in a portal-based system and shows highly accurate estimates of dielectric constant for dielectric objects placed on high conductivity skin surfaces, even for very low permittivity values. Validation with measurements has been also presented. The importance of this processing method is clear in the context of the identification of concealed explosive related threats or contraband by using millimeter-wave based scanners. Furthermore, the method is based on the use of non-ionizing frequencies and conventional RF hardware, providing a safe, non-costly solution for non-metallic threats identification.

ACKNOWLEDGMENT

This work is supported by CenSSIS, the Gordon Center for Subsurface Sensing and Imaging Systems NSF ERC Program (Award number EEC-9986821); by the Ministerio de Ciencia e Innovación of Spain/FEDER under projects CONSOLIDER-INGENIO CSD2008-00068 (TERASENSE) and TEC2011-24492/TEC (iSCAT); by PCTI Asturias under project IPT-2011-0951-390000 (TECNIGRAF). This material is based upon work supported by the Science and Tech. Directorate, U.S. Department of Homeland Security under the Award Number 2008-ST-061-ED0001.

REFERENCES

1. Martínez-Lorenzo, J. A., F. Quivira, and C. M. Rappaport, "SAR imaging of suicide bombers wearing concealed explosive threats," *Progress In Electromagnetics Research*, Vol. 125, 255–272, 2012.
2. Giakos, G. C., M. Pastorino, F. Russo, S. Chowdhury, N. Shah, and W. Davros, "Noninvasive imaging for the new century," *IEEE Instrumentation and Measurement Mag.*, Vol. 2, 32–35, Jun. 1999.
3. Sheen, D. M., D. L. McMakin, and T. E. Hall, "Three-dimensional millimeter-wave imaging for concealed weapon detection," *IEEE Transactions on Microwave Theory and Techniques*, Vol. 49, No. 9, 1581–1592, Sep. 2001.
4. Álvarez, Y., B. Gonzalez-Valdes, J. A. Martínez, F. Las-Heras, and C. M. Rappaport, "3D whole body imaging for detecting explosive-related threats," *IEEE Transactions on Antennas and Propagation*, Vol. 60, No. 9, 4453–4458, Sep. 2012.
5. Fernandes, J., C. M. Rappaport, J. A. Martínez-Lorenzo, and M. Hagelen, "Experimental results for standoff detection of concealed body-worn explosives using millimeter-wave radar and limited view ISAR processing," *2009 IEEE Conference on Technologies for Homeland Security (HST09)*, 456–460, Waltham, MA, May 11–12, 2009.
6. Álvarez, Y., J. A. Martinez, F. Las-Heras, and C. Rappaport, "An inverse fast multipole method for imaging applications," *IEEE Antennas and Wireless Propagation Letters*, Vol. 10, 1259–1262, 2011.
7. Angell, A. and C. Rappaport, "Computational modelling analysis of radar scattering by metallic body-worn explosive devices covered with wrinkled clothing," *2007 IEEE/MTT-S International Microwave Symposium*, 1943–1946, Honolulu, HI, Jun. 3–8, 2007.
8. Cooper, K. B., R. J. Dengler, N. Llombart, B. Thomas, G. Chattopadhyay, and P. H. Siegel, "THz imaging radar for standoff personnel screening," *IEEE Transactions on Terahertz Science and Technology*, Vol. 1, No. 1, 169–182, Sep. 2011.
9. US patent 5181234, Smith, S. W., "X-ray backscatter detection system," Issued 1993-01-19, 1993.
10. Eilbert, R. F. and S. H. Shi, "Improved imaging for X-ray inspection systems," *IEEE Aerospace and Electronic Systems Magazine*, Vol. 20, No. 3, 23–28, 2005.
11. Yinon, J., *Forensic and Environmental Detection of Explosives*. Chichester, John Wiley and Sons, 1999.

12. Leahy-Hoppa, M., M. Fitch, X. Zheng, L. Hayden, and R. Osiander, "Wideband terahertz spectroscopy of explosives," *Chemical Physics Letters*, Vol. 424, No. 8, 227–230, 2007.
13. Cook, D. J., B. K. Decker, and M. G. Allen, "Quantitative THz spectroscopy of explosive materials," *Optical Terahertz Science and Technology Conf.*, Orlando, Florida, Mar. 14–16, 2005.
14. Liu, H., Y. Chen, G. J. Bastiaans, and X. Zhang, "Detection and identification of explosive RDX by THz diffuse reflection spectroscopy," *Optics Express*, Vol. 14, No. 1, 415–423, 2006.
15. Shea, P., T. Gozani, and H. Bozorgmanesh, "A TNA explosives-detection system in airline baggage," *Nuclear Instruments and Methods in Physics Research Section A: Accelerators, Spectrometers, Detectors and Associated Equipment*, Vol. 299, No. 20, 444–448, Dec. 1990.
16. Itozaki, H. and G. Ota, "Nuclear quadrupole resonance for explosive detection," *International Journal on Smart Sensing and Intelligent System*, Vol. 1, No. 3, 705–715, Sep. 2008.
17. Martinez-Lorenzo, J. A., C. M. Rappaport, and F. Quivira, "Physical limitations on detecting tunnels using underground-focusing spotlight synthetic aperture radar," *IEEE Transactions on Geoscience and Remote Sensing*, Vol. 49, No. 1, 65–70, Jan. 2011.
18. Rappaport, C., Q. Dong, E. Bishop, A. Morgenthaler, and M. Kilmer, "Finite difference frequency domain (FDFD) modeling of two dimensional TE wave propagation and scattering," *Proc. URSI Conf.*, 1134–1136, Pisa, Italy, May 16–18, 2004.